

## FIRST HIGH-G MEASUREMENT BY THERMAL ACCELEROMETERS

A. Garraud\*, P. Combette, J.M. Gosalbes, B. Charlot and A. Giani

Institut d'Electronique du Sud - Université Montpellier 2 - CNRS UMR 5412, Montpellier, FRANCE

### ABSTRACT

In the present work, the design and experimental set-up conditions of a micromachined accelerometer based on convection heat transfer are reviewed. The effects on sensitivity are analytically studied and allow discussion of the linearity range. They are confirmed by simulation and experimental results. With optimized experimental parameters, we achieve for the first time high-g measurements of up to 10,000 g with a thermal accelerometer.

### KEYWORDS

Accelerometer, thermal, convection, high-g, MEMS.

### INTRODUCTION

The most common principle of acceleration sensing is based on the movement of a solid proof mass attached with springs to the substrate subjected to an acceleration load. Several transduction mechanisms for the measurement of seismic mass displacements are available including piezoresistivity, piezoelectricity or parallel-plate capacitors. Micro-systems are therefore widely used in consumer electronics, automation for robotic systems and in the automotive industry with crash detection.

In the last fifteen years, a new concept of acceleration sensing with no solid proof mass has been developed. The physical principle is based on a locally heated gas acting as a proof mass. Under acceleration conditions, free-convection transfer is modified and induces the gas motion. It leads to high shock reliability coupled with very competitive performances [1]-[2]. Some previous studies have modeled thermal sensitivity as a function of several parameters such as sensor geometry or gas properties [3]-[6], but to our knowledge, no one presents thermal accelerometers able to measure acceleration ranges as high as several thousand g and gives the parameters to achieve such a linearity range. Such accelerometers can have applications for high-vibration level measures or aerospace engineering.

### SENSOR PRINCIPLE

#### Working principle

The thermal accelerometer described in Fig. 1 is composed of one electrical heating resistor placed symmetrically over a cavity etched on silicon. When the central resistor is powered, it heats up the surrounding gas creating a symmetrical temperature distribution under no acceleration conditions as illustrated in Fig. 2 by the straight line. Two thermal detectors placed on each side of the heater provide similar electrical outputs. If the sensor is subjected to an acceleration  $\Gamma$ , the balance in

free-convection transfer is modified as shown in Fig. 2 with the dash line and a temperature difference  $\delta T$  appears between the two detectors, linked to  $\Gamma$  whereby sensitivity  $S$  equals  $\delta T/\Gamma$ .

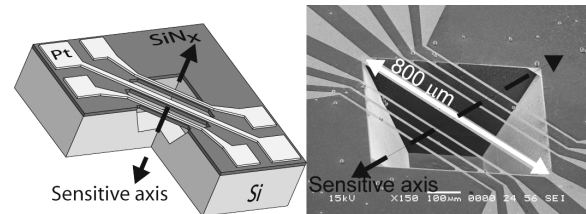


Figure 1: Schematic diagram of a simple micromachined thermal accelerometer and Scanning Electron Microscope (SEM) image of a micromachined sensor with three pairs of detectors.

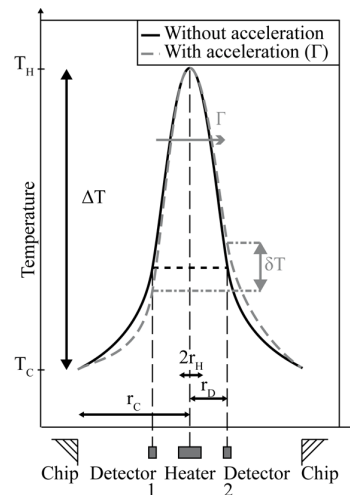


Figure 2: Gas temperature distribution along the sensitive axis, without (straight line) and with (dash) acceleration.

### Microstructure design

Figure 1 shows an SEM image of a device with three pairs of suspended detectors on either side of the heater resistor. Every thin-film platinum bridge is made of a 500-nm low stress silicon nitride membrane ( $\text{SiN}_x$ ) [5] covered by a 300-nm platinum layer including a Cr-adhesion layer. The  $\text{SiN}_x$  layer has been chosen for its low-stress level allowing flat-standing structures. Platinum is electron-beam evaporated at 400 °C and vacuum-annealed at 500 °C. The platinum resistors and  $\text{SiN}_x$  layer are successively patterned by a Corial 200 IL Reactive Ion Etching (RIE) device. The cavity is then obtained with KOH wet anisotropic etching of the (100) oriented silicon and provides thermal isolation.

## MODELING AND INSTRUMENTATION

### Analytical model of sensitivity

The thermal accelerometer is based on heat transfer exchanges and in particular on free convection heat transfer in a gas contained in a closed chamber. Effects of viscous and compression heating are neglected and all gas properties except density are considered constant with temperature (Boussinesq approximation). The sensor shape is modelled as two concentric circular cylinders: the inner is kept at a temperature  $T_H$  with a radius  $r_H$ , the outer is kept at a temperature  $T_C$ , with  $T_C < T_H$ , and has a radius  $r_C$ . An analytical study using this high degree of symmetry [6][8] has allowed understanding of the behavior of thermal sensitivity  $S$  as a function of thermo-physical gas parameters, experimental set-up and design. Thereby, the sensor sensitivity can be expressed as:

$$S = \frac{\delta T}{\Gamma} \propto \frac{\rho^2 \cdot \beta \cdot C_P}{\mu \cdot \lambda} \cdot \Delta T^2 \cdot r_H^3 \cdot f(r_D, R) \quad (1)$$

With  $\rho$  gas density,  $\beta$  thermal expansion,  $C_P$  specific heat,  $\mu$  dynamic viscosity,  $\lambda$  thermal conductivity,  $\Delta T$  temperature difference between the heater and the substrate,  $r_H$  radius equivalent to half-width of the heater resistor and  $f(r_D, R)$  a typical geometrical dimensionless function of the sensor geometry dependent on the detector position  $r_D$  and on the ratio  $R$  of half-width of the cavity  $r_C$  to  $r_H$ . It can be analytically shown that this function is proportional to  $r_C^3$ .

### Numerical simulations

Numerical simulations are carried out using a commercially available finite volume code software Fluent<sup>®</sup> 6.2. Equations concerning density, momentum and energy were spatially discretized by means of a fully implicit third order finite volume method conceived from the original MUSCL scheme (Monotone Upstream-Centered Schemes for Conservation Laws). Pressure discretization was performed by means of a Body Force Weighted scheme. The array meshing is adjusted to improve the density of calculation near the critical regions. The fluid model that we used is an ideal gas taking into account the variations of  $\mu$ ,  $\lambda$ ,  $C_P$  according to the temperature using a polynomial profile. The initial values for velocity, temperature and viscosity fields are set to constant values over the entire computational range. A computational grid of 40,000 cells used for calculations represents the gas inside the cavity. The solver undertakes iteration until the convergence criterion is satisfied, taking scaled residuals of the modified variables in the governing equations as a measure. Calculations were also conducted with a larger number of cells which led to longer time computation without significant reduction of residuals. In order to obtain a grid-independent solution, a particular isothermal wall heat flux is monitored for convergence until it reaches less than a 0.01 % variation between iterations.

### Measuring methods

Since thermal detectors are made of platinum, they are sensitive to temperature modification due to resistance variation. The platinum layer resistivity is about  $15 \mu\Omega \cdot \text{cm}$  with a temperature coefficient of resistance close to  $3.1 \times 10^{-3} \text{ }^\circ\text{C}^{-1}$ .

First estimations of thermal sensitivity are obtained from a multi-position test bench: acceleration of gravity is linked to the output value, i.e. sensitivity value in this case.

To measure the sensor linearity range, we use a centrifuge which attains 10,000 g and an autonomous data-recorder electronic circuit, both illustrated in Fig. 3. Mechanical balance is performed with a second unplugged thermal accelerometer diametrically opposite to the active one.

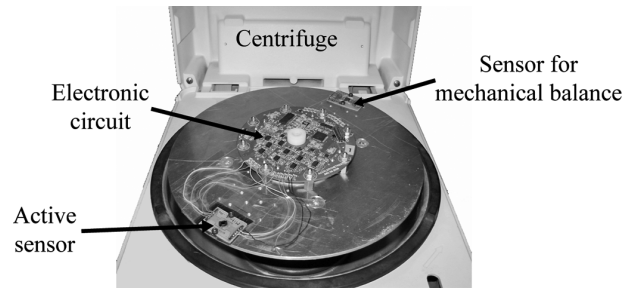


Figure 3: Centrifuge with autonomous data-recorder electronic circuit connected to a thermal accelerometer.

## CHOICE OF PARAMETERS

### Choice of cavity size

For the same temperature profile height, a non-linearity boundary appears for higher acceleration ranges when less gaseous mass is present in the cavity. A method of reducing this state is to decrease cavity width. We can deduce with relation (1) that this condition will induce a lower thermal sensitivity. In order to confirm this fact, we experimentally measure thermal sensitivity for several sensors with different cavity widths. The results are shown in Fig. 4: sensitivity increases with the cavity width with slope 3 in a log-log scale, as does the geometrical function  $f(r_D, R)$ .

Therefore, one of the parameters necessary to obtain a wide linearity range is to use a small-size gas cavity.

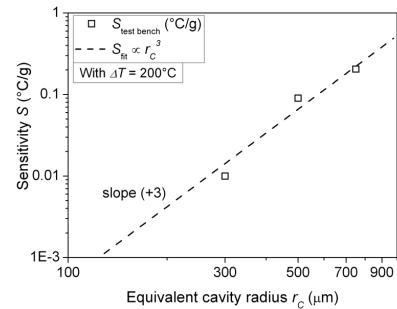


Figure 4: Experimental sensitivity and fitted curve versus equivalent cavity radius, multi-position test bench data.

### Choice of temperature profile height $\Delta T$

Each parameter in relation (1) has to be adjusted to obtain a minimal sensitivity value in order to obtain a large linearity range. One of these parameters is the temperature difference between the heater and the chip, linked to the electrical power injected into the heating resistor. By increasing step by step the current injected into the heater, we monitor the sensitivity behavior, as shown in Fig. 5: sensitivity increases with the square of the temperature difference  $\Delta T$ , as predicted by relation (1). Thus we can conclude that this relation is true even at small scales. Moreover, this implies that the electrical injected power has to be adapted. On one hand, high temperatures on the heater would damage the thermoresistive properties of the Pt layer and consequently sensor performance. On the other hand, a low temperature difference between heater and chip would make the sensor more sensitive to noise. Therefore, a temperature difference height  $\Delta T$  equal to 200 °C is chosen for the following studies.

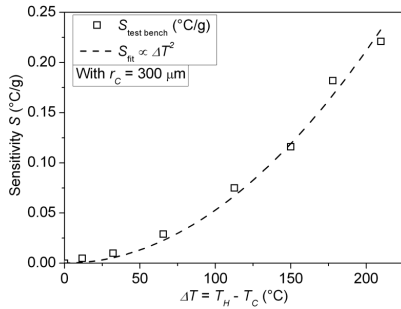


Figure 5: Experimental sensitivity and fitted function versus the temperature profile height, multi-position test bench data.

## RESULTS

### Simulation contribution

As mentioned above, this present study is strengthened by finite-element simulations that outline thermal sensitivity behavior versus acceleration for different equivalent cavity radii as illustrated with Fig. 6. In this way the analytical theory is confirmed: the smaller the cavity, the more linearity range is predicted to be attained, until 100,000 g for very low-size sensors ( $r_C = 94 \mu\text{m}$ ).

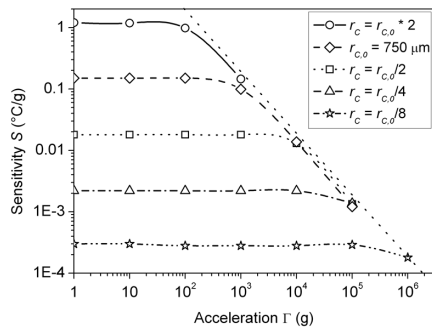


Figure 6: Simulated thermal sensitivity versus acceleration for different cavity sizes,  $r_C$ .

### Effect of sensor size on linearity range

To experimentally compare their actual linearity range, we subjected thermal accelerometers with different cavity sizes to accelerations of up to 3,000 g using the centrifuge and autonomous data-recorder electronic circuit. The results are presented in Fig. 7 and this figure can be seen as a rewriting of Fig. 4. Saturation is reached for accelerations higher than 500 g on the sensor with a cavity larger than  $r_C = 500 \mu\text{m}$  while the sensor with  $r_C = 300 \mu\text{m}$  remains linear until 3,000 g. These experimental results confirm both analytical and numerical conclusions.

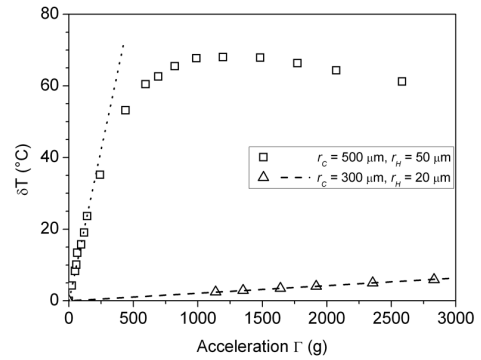


Figure 7: Experimental tests of linearity range for different cavity sizes,  $r_C$ .

### Impact of detectors distance from the heater, $r_D$

Previous studies [3][4] have shown that the distance of detectors from the heater has an influence on sensitivity. Using the accelerometer shown on Fig. 1, we tested the detector pairs for an acceleration range up to 3,000 g to focus only on the effect on sensitivity. Figure 8 highlights the influence of  $r_D$  on sensitivity for a 600- $\mu\text{m}$  cavity width. In this case, sensitivity decreases with the distance from the heater:  $S$  varies from a factor 2 with the position. Nevertheless no consequence about the effect on linearity range can be extracted from this graph.

In conclusion, even if a lower sensitivity is needed, for a given cavity size, the larger value has to be chosen to have the highest signal-to-noise ratio.

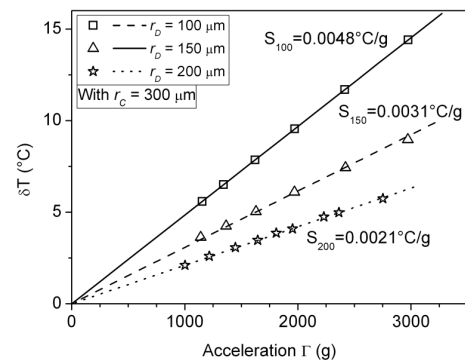


Figure 8: Experimental linearity range for different detector distances from the heater,  $r_D$ , with  $r_C = 300 \mu\text{m}$ .

## HIGH G MEASUREMENT

The different studies allow us to choose the most appropriate parameters to obtain a large linearity range: cavity size, detector position in the cavity and also experimental set-up with the electrical power injected into the heater to create the temperature profile. The sensor optimized in this way is then placed into the centrifuge and subjected to accelerations of up to 10,000 g as shown in Fig. 9. We deduce from this test that the 600- $\mu\text{m}$  width thermal accelerometer is still linear at 10,000 g with a linearity error lower than 4 %.

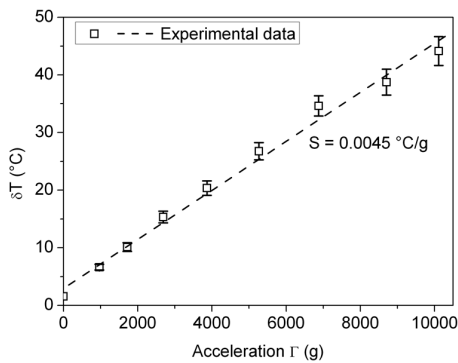


Figure 9: Experimental high-g measurement with optimized parameters.

## CONCLUSION

This work investigates the linearity range characterization of accelerometers based on convection heat transfer. The first parameters adjusted concern the sensor geometry. The whole system size is reduced from an equivalent cavity radius  $r_C = 750 \mu\text{m}$  to  $r_C = 300 \mu\text{m}$ . The distance from the heater to the detectors is also adapted to the reduced size and the detectors are placed at one third of the cavity half-width to optimize the value of sensitivity and reduce noise contribution. The temperature profile height  $\Delta T$  is chosen in the same manner. Finally, with the aforementioned parameters adjusted, our thermal accelerometer is the first able to measure high-g accelerations and we prove its linearity

range up to 10,000 g.

## REFERENCES

- [1] A.M. Leung, J. Jones, E. Czyzewska, J. Chen and M. Pascal, "Micromachined accelerometer with no proof mass," *Digest Tech. Papers International Electron Devices Meeting, Conference, Washington, DC, USA*, December 7–10, 1997, pp. 899–902.
- [2] X.B. Luo, Y.J. Yang, F. Zheng, Z.X. Li and Z.Y. Guo, "An optimized micromachined convective accelerometer with no proof mass," *J Micromech Microeng*, Vol. 11, no. 5, pp. 504–508, 2001.
- [3] F. Mailly, A. Martinez, A. Giani, F. Pascal-Delanoy and A. Boyer, "Effect of gas pressure on the sensitivity of a micromachined thermal accelerometer", *Sensor Actuat A-Phys*, Vol. 109, pp. 88-94, 2003.
- [4] F. Mailly, A. Martinez, A. Giani, F. Pascal-Delanoy and A. Boyer, "Design of a micromachined thermal accelerometer: thermal simulation and experimental results", *Microelectr J*, Vol. 34, pp.275-280, 2003.
- [5] J. Courteaud, P. Combette, N. Crespy, G. Cathebras and A. Giani, "Thermal simulation and experimental results of a micromachined thermal inclinometer", *Sensor Actuat A-Phys*, Vol. 141, pp. 307–313, 2008.
- [6] A. Garraud, P. Combette, F. Pichot, J. Courteaud, B. Charlot and A. Giani, "Frequency response analysis of an accelerometer based on thermal convection", *J. Micromech. Microeng.* Vol. 21, no. 3, pp. 035017, 2011.
- [7] P. Temple-Boyer, C. Rossi, E. Saint-Etienne and E. Scheid, "Residual stress in low pressure chemical vapor deposition SiNx films deposited from silane and ammonia", *J Vac Sci Technol A*, Vol. 16, No. 4, pp. 2003-2007, 1998.
- [8] P. Hodnett, "Natural convection between horizontal heated concentric circular cylinders", *J Appl Math Phys*, Vol. 24, pp. 507-516, 1973.

## CONTACT

\*A.GARRAUD, tel: 33-04-67-14-37-13;  
alexandra.garraud@ies.univ-montp2.fr